

Comparing linear ion-temperature-gradient-driven mode stability of the National Compact Stellarator Experiment and a shaped tokamak

J. A. Baumgaertel, G. W. Hammett, and D. R. Mikkelsen

Citation: *Phys. Plasmas* **20**, 022305 (2013); doi: 10.1063/1.4791657

View online: <http://dx.doi.org/10.1063/1.4791657>

View Table of Contents: <http://pop.aip.org/resource/1/PHPAEN/v20/i2>

Published by the [American Institute of Physics](#).

Related Articles

Modelling of radiative divertor operation towards detachment in experimental advanced superconducting tokamak

Phys. Plasmas **20**, 022311 (2013)

Identification and control of plasma vertical position using neural network in Damavand tokamak

Rev. Sci. Instrum. **84**, 023504 (2013)

On the toroidal plasma rotations induced by lower hybrid waves

Phys. Plasmas **20**, 022502 (2013)

Quick asymptotic expansion aided by a variational principle

Phys. Plasmas **20**, 024504 (2013)

Ion temperature gradient instability at sub-Larmor radius scales with non-zero ballooning angle

Phys. Plasmas **20**, 022101 (2013)

Additional information on Phys. Plasmas

Journal Homepage: <http://pop.aip.org/>

Journal Information: http://pop.aip.org/about/about_the_journal

Top downloads: http://pop.aip.org/features/most_downloaded

Information for Authors: <http://pop.aip.org/authors>

ADVERTISEMENT



AIP Advances

Special Topic Section:
PHYSICS OF CANCER

Why cancer? Why physics? [View Articles Now](#)

Comparing linear ion-temperature-gradient-driven mode stability of the National Compact Stellarator Experiment and a shaped tokamak

J. A. Baumgaertel,¹ G. W. Hammett,² and D. R. Mikkelsen²

¹Los Alamos National Laboratory, Los Alamos, New Mexico 87544, USA

²Princeton Plasma Physics Laboratory, Princeton, New Jersey 08543, USA

(Received 24 October 2012; accepted 23 January 2013; published online 11 February 2013)

One metric for comparing confinement properties of different magnetic fusion energy configurations is the linear critical gradient of drift wave modes. The critical gradient scale length determines the ratio of the core to pedestal temperature when a plasma is limited to marginal stability in the plasma core. The gyrokinetic turbulence code GS2 was used to calculate critical temperature gradients for the linear, collisionless ion temperature gradient (ITG) mode in the National Compact Stellarator Experiment (NCSX) and a prototypical shaped tokamak, based on the profiles of a JET H-mode shot and the stronger shaping of ARIES-AT. While a concern was that the narrow cross section of NCSX at some toroidal locations would result in steep gradients that drive instabilities more easily, it is found that other stabilizing effects of the stellarator configuration offset this so that the normalized critical gradients for NCSX are competitive with or even better than for the tokamak. For the adiabatic ITG mode, NCSX and the tokamak had similar adiabatic ITG mode critical gradients, although beyond marginal stability, NCSX had larger growth rates. However, for the kinetic ITG mode, NCSX had a higher critical gradient and lower growth rates until $a/L_T \approx 1.5 a/L_{T,crit}$, when it surpassed the tokamak's. A discussion of the results presented with respect to a/L_T vs. R/L_T is included. © 2013 American Institute of Physics. [<http://dx.doi.org/10.1063/1.4791657>]

I. INTRODUCTION

Two of the main magnetic fusion energy designs are the axisymmetric tokamak and the non-axisymmetric stellarator. Tokamaks have seen significant heat loss due to turbulence,¹ while stellarator losses have traditionally been dominated by their larger neoclassical transport. Studying turbulent transport in stellarators is increasingly important, however, as modern stellarator designs (such as Wendelstein 7-AS (W7-AS),² Wendelstein 7-X (W7-X),^{3,4} the National Compact Stellarator Experiment (NCSX),⁵ the Large Helical Device (LHD),⁶ and the Helically Symmetric Experiment (HSX)⁷⁻⁹) have shown or are designed to have improved neoclassical confinement and stability properties. Therefore, turbulence could be increasingly relevant in stellarator experiments. Several gyrokinetic studies of drift-wave-driven turbulence in stellarator geometry have been done¹⁰⁻²⁶ with a variety of gyrokinetic codes, such as GS2,²⁷ GENE,^{15,28} GKV-X,^{16,17} and FULL.¹⁰ These codes have all been linearly benchmarked against each other for non-axisymmetric geometries.^{18,19} Progress has even been made in optimizing stellarator designs to have reduced turbulent transport.²⁹

Besides comparing good stellarator configurations (as was done in Refs. 19, 21, and 29), one would like to compare stellarator confinement with that of tokamaks. The relative benefits of each device are important to consider when designing the next generation of experiments. A few previous comparison studies have been done, such as those in Refs. 20 and 21. Here, the gyrokinetic turbulence code GS2 (Ref. 27) is used to compare microinstability of the electrostatic adiabatic ion temperature gradient (ITG) and the electrostatic collisionless kinetic ITG modes in the quasi-axisymmetric NCSX design to that of a highly elongated

tokamak. Because this tokamak and NCSX geometry differ so significantly, it is hard to pinpoint what parameter has the greatest effect, but overall effects will be examined.

ITG mode-driven turbulence has been connected experimentally to measure heat losses in both tokamaks (e.g., Ref. 30) and the LHD.²² There is much variability in stellarator designs, and it is unclear without more study which modes will dominate in each. Preliminarily, Ref. 31 suggests that ITG transport in NCSX may be larger than that of ETG (see Figs. 8 and 9 of that paper). While only the ITG mode thresholds are compared in this paper, further study could show that other modes dominate in this case and in other devices.

In Sec. II, a simple comparison metric is defined for use in this paper. Sections II A and II B describe the tokamak and stellarator configurations: a Miller equilibrium for the highly elongated tokamak and a numerical equilibrium for NCSX. Next, growth rates and critical temperature gradients are compared for the ITG mode in Secs. II C and II D. Finally, the study is concluded in Sec. III.

II. NCSX VS. A SHAPED TOKAMAK

To understand the trade-offs between stellarator and axisymmetric geometry and their confinement capabilities, designs can be compared computationally. One metric of confinement quality is the ratio of the core temperature to the pedestal temperature, T_0/T_{ped} , as fusion reactors need very high core temperatures, and high core temperature implies good confinement. This ratio is related to the critical temperature gradients. If $-\partial T/\partial r \approx T/L_{T,crit}$, temperature-gradient-driven instabilities are marginally stable—a reasonable assumption in a reactor plasma, as temperatures inside

the pedestal will be so high that profile stiffness will ensure that gradients are close to marginal stability. This is demonstrated by Fig. 3 of Ref. 32, which shows that fusion power (and thus the temperature profile) depends primarily on the pedestal temperature and not the beam power, for the case of balanced beams.

At marginal stability (assuming $1/L_{T,crit}$ is independent of minor radius)

$$T(r) = T_0 e^{-r/L_{T,crit}}. \quad (1)$$

The minimum temperature is at the edge where r is maximum, $r_{max} = a$, where a is the minor radius. In this simplified story, another approximation will be made that T_{ped} occurs at $r = a$. So, $T(a) = T_{ped} = T_0 e^{-a/L_{T,crit}}$. Therefore, the core temperature's dependence on the critical temperature gradient for typical tokamak values^{33–35} of $a/R \approx 1/3.5$ and $R/L_{T,crit} \approx 5$ is

$$\begin{aligned} T_0/T_{ped} &= e^{a/L_{T,crit}} \\ &= e^{(a/R)(R/L_{T,crit})} \\ &\approx e^{(1/3.5)5} \approx 4.2. \end{aligned} \quad (2)$$

One wants to maximize the core temperature, T_0 . T_{ped} is set by non-transport mechanisms and cannot be arbitrarily high, leaving $a/L_{T,crit}$ as the important parameter in Eq. (2). If an alternative fusion device design could increase $a/L_{T,crit}$ by just 30%, this would increase the central temperature by 50%, more than double the fusion power (a caveat—this is a simple estimate and does not take into account the fact that MHD stability changes with higher pressure peakedness). In this paper, the critical ion temperature gradients are compared for NCSX and a strongly shaped tokamak design. The stated stellarator minor and major radii are the average values.

A. Miller equilibrium for this tokamak

NCSX runs were compared to a potential high-elongation tokamak based on a composite of ARIES-AT³⁶ and JET H-mode shot #52979. It is well known that tokamak performance improves at high elongation and triangularity^{37–39} (in large part because this leads to more plasma current at fixed q), so when designing future tokamaks, one would like to use the highest possible values of elongation and triangularity, although elongation is limited by vertical stability control if it becomes too large. Some initial studies of shaping effects with GS2 were carried out in Ref. 35, using a range of shapes scaled from the particular JET shot #52979 (available in the ITER profile database⁴⁰). This JET shot, described in more detail in Refs. 41 and 42, was chosen as a representative H-mode plasma that has been studied in detail by gyrokinetics codes before. Parameters for this paper were chosen from shot #52979, but the shaping parameters were scaled to the higher levels achievable in tokamaks. These values of edge elongation and triangularity are from ARIES-AT, which generally tried to maximize these parameters subject to engineering and vertical stability constraints. This JET shot has a conventional q profile, while the ARIES-AT design study assumed that a

reversed shear scenario can be stably maintained in steady state. The composite tokamak of this paper has a conventional q profile. The Miller equilibrium⁴³ for this prototypical or generic strongly shaped tokamak was set up in the following way.

The shaping study in Ref. 35 chose to focus on the radius $r/a = 0.8$ in order to be fairly near the plasma edge where shaping effects are stronger, but not too far out because gyrokinetic codes often do not compare well with the experiments near the edge (perhaps, because edge turbulence is driven by mechanisms other than ITG/TEM modes that require higher resolution than usual or additional effects that are not included in present gyrokinetic codes). Therefore, the study in this section uses $r/a = 0.8$.

Just inside the separatrix at the 95% poloidal flux surface, the JET shot had an elongation of $\kappa_{95} = 1.73$ and triangularity of $\delta_{95} = 0.46$, while the core elongation is $\kappa_{core} \approx 1.3$. At the radius of interest, $r/a = 0.8$, $R/a = 3.42$, $\kappa_{0.8} = 1.46$, $\kappa'_{0.8} = 0.57$, $\delta_{0.8} = 0.19$, $\delta'_{0.8} = 0.60$, and the Shafranov shift is $\partial R_0/\partial r = -0.14$. Finally, the safety factor $q_{0.8} = 2.03$ and magnetic shear $\hat{s} = 1.62$.

Keeping JET's Shafranov shift, q and \hat{s} , a modified ARIES-AT case was created using its $\kappa_{95} = 2.08$ and $\delta_{95} = 0.76$. Assuming, from the tokamak shaping studies, that $\kappa, \kappa' \propto (\kappa_{95} - \kappa_{core})$ and $\delta, \delta' \propto \delta_{95}$,

$$\kappa_{0.8}^{tok} = \kappa_{core}^{JET} + \left(\kappa_{0.8,JET} - \kappa_{core}^{JET} \right) \frac{(\kappa_{95,tok} - \kappa_{core}^{JET})}{(\kappa_{95,JET} - \kappa_{core}^{JET})} = 1.59, \quad (3)$$

$$\kappa'_{0.8}^{tok} = \kappa_{0.8}^{JET'} \frac{(\kappa_{95,tok} - \kappa_{core}^{JET})}{(\kappa_{95,JET} - \kappa_{core}^{JET})} = 1.03, \quad (4)$$

$$\delta_{0.8}^{tok} = \delta_{0.8}^{JET} \frac{\delta_{95}^{tok}}{\delta_{95}^{JET}} = 0.31, \quad (5)$$

$$\delta'_{0.8}^{tok} = \delta'_{0.8}^{JET'} \frac{\delta_{95}^{tok}}{\delta_{95}^{JET}} = 0.99. \quad (6)$$

Representative flux surfaces for this prototype strongly shaped tokamak are shown in Figure 1.

B. NCSX geometry

References 18 and 44 describe how non-axisymmetric geometry input is created for GS2. The coordinate system of the flux-tube code GS2 includes the radial coordinate, $\rho = \sqrt{s}$ ($s \approx (r/a)^2$ is the normalized toroidal flux), the coordinate aligned to the field line, θ , and the angle that selects a flux tube, $\alpha = \zeta - q(\theta - \theta_0)$ (where ζ and θ are Boozer toroidal and Boozer poloidal coordinates and θ_0 is the ballooning parameter).

The GS2 documentation⁴⁵ defines geometrical quantities in terms of a parameter $d\Psi_N/d\rho$, where ρ is the radial coordinate and Ψ_N is the normalized poloidal flux. Geometrical quantities in this paper follow GS2 notation and include $d\Psi_N/d\rho$. For more information, see Refs. 18 and 44.

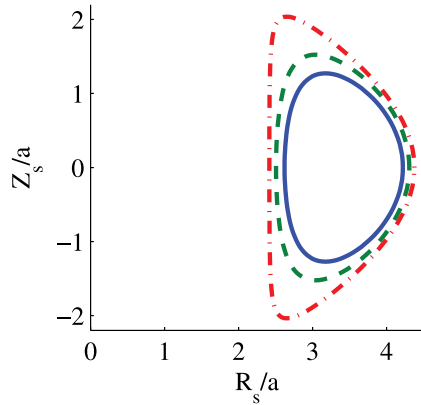


FIG. 1. Illustration of flux surface shapes for a prototypical strongly-shaped tokamak at $r/a=0.8$ (blue solid line), 0.9 (green dashed line), and 0.98 (red dash-dot line).

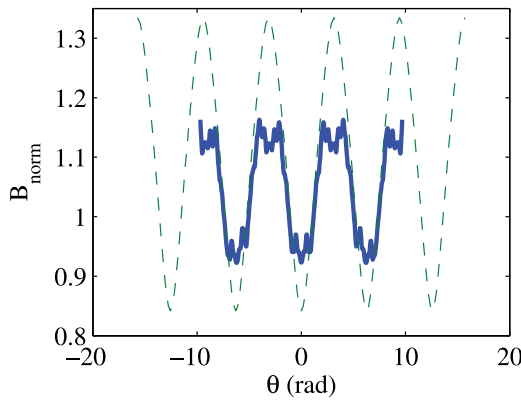


FIG. 2. The NCSX (blue solid line) and tokamak (green dashed line) equilibria: normalized $|B|$ vs. θ .

Figures 2–4 show the magnitude of the magnetic field, curvature drift, and $(|k_{\perp}|/k_{\theta})^2$ for both the tokamak and NCSX field line over the entire domain, and Figs. 5–7 show close-ups around $\theta = 0$. See Table I for a complete list of geometrical quantities and their values.

Notice that the bad (positive) curvature regions of NCSX are much more localized than the tokamak case. Coupled with the much stronger local magnetic shear (responsible for the sharp peaks in $k_{\perp} \propto \hat{s}$ (Fig. 6)), this

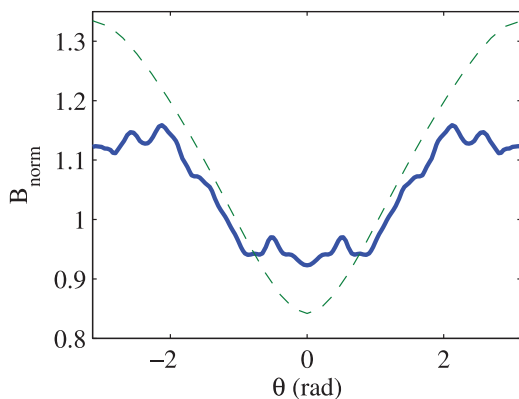


FIG. 3. The NCSX (blue solid line) and tokamak (green dashed line) equilibria: normalized $|B|$ vs. θ , showing a close-up around $\theta = 0$.

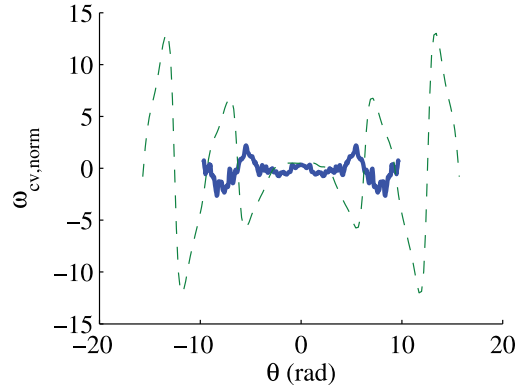


FIG. 4. The NCSX (blue solid line) and tokamak (green dashed line) the curvature drift frequency ($\omega_{cv, norm} = (2a^2/B_N)(d\Psi_N/d\rho)(k_{\perp}/n) \cdot \mathbf{b} \times [\mathbf{b} \cdot \nabla \mathbf{b}]$) along θ .

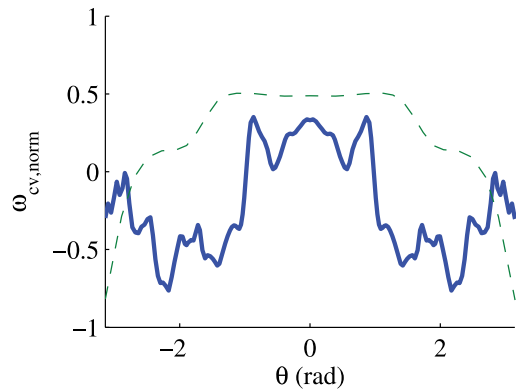


FIG. 5. The NCSX (blue solid line) and tokamak (green dashed line) equilibria: the curvature drift frequency ($\omega_{cv, norm} = (2a^2/B_N)(d\Psi_N/d\rho)(k_{\perp}/n) \cdot \mathbf{b} \times [\mathbf{b} \cdot \nabla \mathbf{b}]$) along θ , showing a close-up around $\theta = 0$.

explains why NCSX’s electrostatic potential eigenfunctions are also more localized than the tokamak’s. An example is shown in Figure 8. These traits could predict better transport properties for NCSX.

C. ITG mode with adiabatic electrons

For the initial study, the ITG mode with adiabatic electrons growth rates and their dependence on temperature

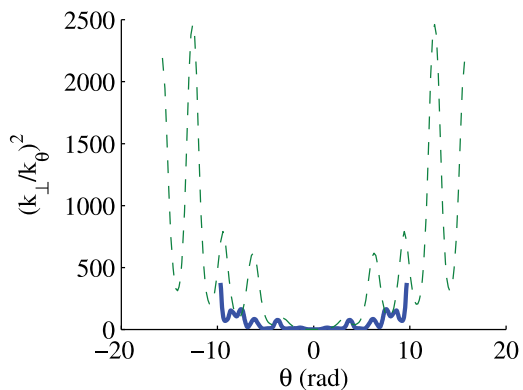


FIG. 6. The NCSX (blue solid line) and tokamak (green dashed line) equilibria: $(\frac{k_{\perp}}{k_{\theta}})^2$ vs. θ .

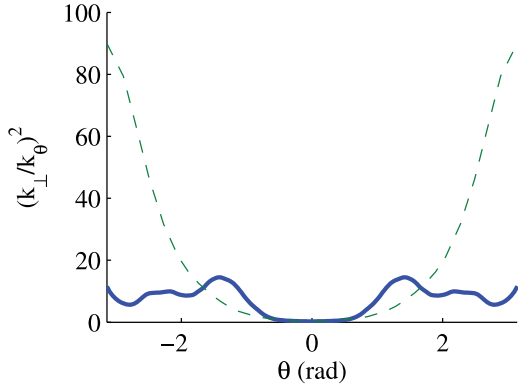


FIG. 7. The NCSX (blue solid line) and tokamak (green dashed line) equilibria: $(\frac{k_{\perp}}{k_{\theta}})^2$ vs. θ , showing a close-up around $\theta = 0$.

TABLE I. Geometry values for the NCSX equilibrium.

Parameter	Value
r/a	0.8
$s \approx (\langle r/a \rangle)^2$	0.64
$\alpha = \zeta - q\theta$	0
θ_0	0
q_s	1.70
\hat{s}	0.835
$\langle \beta \rangle$	0.0%
R	$\approx 4.7a_N \approx 1.5$ m
a_N	≈ 0.322 m
$B_a = \langle B \rangle$	1.58 T

gradient were compared. Figures 9 and 10 show typical growth rate spectra for NCSX and this tokamak. In Figure 11, the growth rate at each a/L_T ($a/L_{Te} = a/L_{Ti}$) was the highest in the range $k_y \rho_i \in [0.2, 1.4]$ for NCSX and $k_y \rho_i \in [0.1, 1.0]$ for the tokamak. These ranges were wide enough to capture the peak of the growth rate spectrum. Growth rates shown are normalized such that $(\gamma, \omega) = (\gamma_{physical}, \omega_{physical})(a/v_{thi})$. The NCSX threshold is $a/L_{T,crit} \approx 1.26$ and the tokamak's is $a/L_{T,crit} \approx 1.22$. This difference is not very significant. However, soon after the threshold, the NCSX growth rates surpass those of the tokamak, indicating that for a given a/L_T , the adiabatic ITG mode is more unstable in NCSX than in the tokamak. This

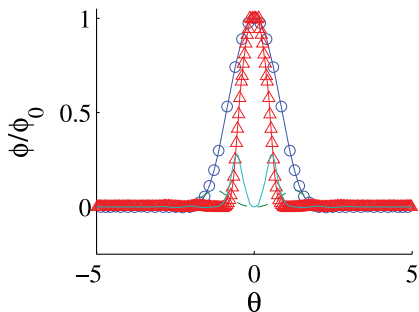


FIG. 8. Comparing electrostatic eigenfunctions for NCSX ($Re(\phi)$: red triangles and $Im(\phi)$: light blue solid line) and tokamak ($Re(\phi)$: blue circles and $Im(\phi)$: green dashed line), for an adiabatic ITG mode with $a/L_T = 3, a/L_n = 0$. For ARIES, $k_y \rho_i = 0.55$, and for NCSX, $k_y \rho_i = 1.0$.

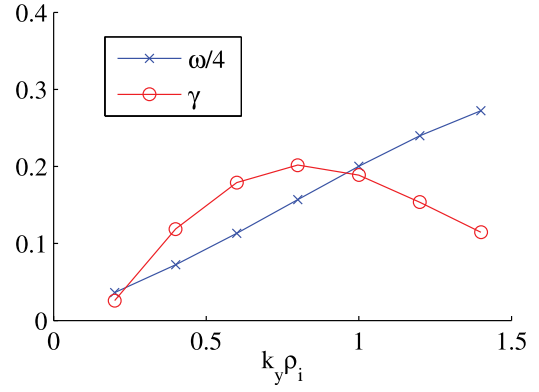


FIG. 9. NCSX growth rate spectrum for the adiabatic ITG mode with $a/L_T = 3, a/L_n = 0$.

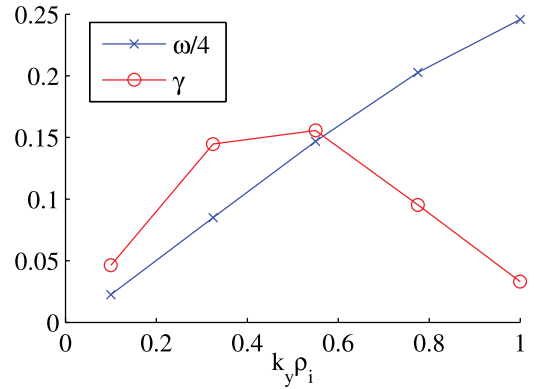


FIG. 10. Tokamak growth rate spectrum for the adiabatic ITG mode with $a/L_T = 3, a/L_n = 0$.

implies that the transport due to the adiabatic ITG mode would be stiffer, but the temperature gradients would still be expected to be very similar since they would be set by $a/L_{T,crit}$.

D. ITG mode with kinetic electrons

The threshold of the ITG mode with kinetic electrons (with $a/L_n = 0$) for the tokamak was somewhat lower than that of NCSX, but the slope of the growth-rate curve is almost the same for both (Fig. 12). Similar to Sec. II C, growth rates shown were the highest on a spectrum of $k_y \rho_i \in$

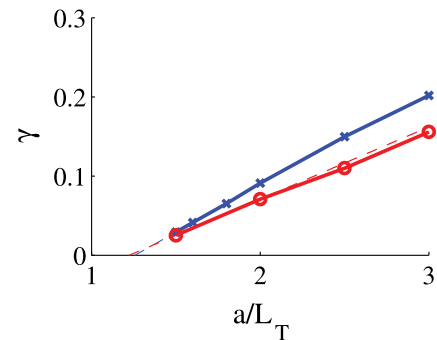


FIG. 11. NCSX (blue crosses) and ARIES-AT-like tokamak (red circles) adiabatic ITG mode growth rate dependence on temperature gradient. Fits obtained through piecewise linear interpolation on the lowest half of the growth rate curve.

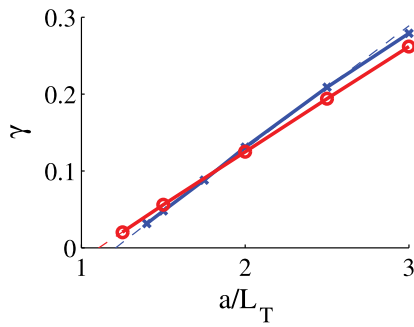


FIG. 12. Growth rates for an ITG mode with kinetic electrons as a function of temperature gradient for NCSX (blue crosses) and an ARIES-AT-like tokamak configuration (red circles). Fits obtained through piecewise linear interpolation on the lowest half of the growth rate curve.

[0.2, 1.4] for NCSX and $k_y \rho_i \in [0.1, 1.0]$ for the tokamak (see Figures 13 and 14 show typical growth rate spectra). With kinetic electrons, the growth rates for the ITG mode in NCSX increased over the adiabatic electron case (Fig. 11), while the critical gradient lowered to $a/L_{T,crit} \approx 1.21$. The tokamak threshold decreased somewhat further, to $a/L_{T,crit} \approx 1.11$. The slope of the NCSX line is somewhat steeper, and for $a/L_T \approx 1.82$, the NCSX growth rates are larger than the tokamak growth rates.

The growth rate vs. a/L_T plot in Figure 12 shows improvement in the a/L_T threshold of NCSX over this tokamak by about 10%. Based on the marginal stability logic in the beginning of Sec. II, this corresponds to about 22% more fusion power for a NCSX-based design relative to the tokamak (with the same edge temperature and density assumed for the two designs, and approximating the fusion power as scaling as T^2). Effects that might change this result include finite beta modifications to the equilibrium and the nonlinear Dimits shift,^{33,35} which could increase each critical gradient, but the required nonlinear simulations are beyond the scope of this work. A Dimits shift has been reported for a stellarator¹⁵ and has been found in tokamak simulations.^{46,47}

This is much better than one might have initially guessed based on just the local value of R/L_T in NCSX vs. a tokamak. While from Eq. (2) it is clear that a/L_T is the relevant parameter for determining the core temperature, in the axisymmetric community the threshold for the ITG instability is usually expressed in terms of R/L_T , which is often the

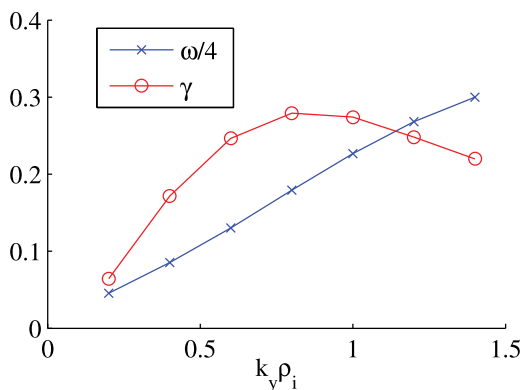


FIG. 13. NCSX growth rate spectrum for the kinetic ITG mode with $a/L_T = 3$, $a/L_n = 0$.

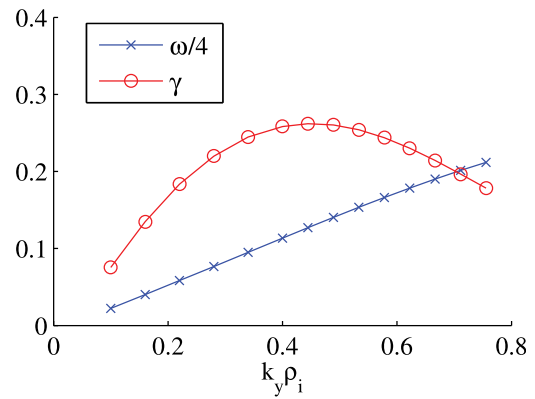


FIG. 14. Tokamak growth rate spectrum for the kinetic ITG mode with $a/L_T = 3$, $a/L_n = 0$.

key parameter numerically. An instability threshold $R/L_{T,crit}$ can be derived from the dispersion relation for a local ITG mode in the bad curvature region, ignoring the parallel dynamics. In this limit, the critical instability parameter is the ratio of the temperature-gradient diamagnetic drift frequency ($\omega_{*T} \propto 1/L_T$) to the curvature drift frequency ($\omega_d \propto 1/R$) (particles with different energies have different curvature drift velocities, which can result in Landau damping. This criterion essentially says that the drive from the temperature gradient must be strong enough to overcome this damping in order to drive instabilities).

A concern could be that if an NCSX design is limited to the same local $R_{loc}/L_{T,loc}$ as in a tokamak, it would have a much lower a/L_T (because at some toroidal locations, such as the left panel of Figure 15, the cross section of NCSX is very narrow, with a local plasma half-width $a_{loc} \approx a/2.58$), and thus would have much lower fusion power. Therefore, the local value of the logarithmic gradient, $1/L_{T,loc} = |\nabla T|/T = (a/L_T)/a_{loc}$, is much larger than the average $1/L_T$. This is enhanced by the larger average aspect ratio $(R/a)_{NCSX} = 4.7$ relative to the tokamak $(R/a)_{tok} = 3.42$ and is partially compensated by the fact that the local radius of curvature of the magnetic field, $R_{loc} = |\hat{b} \cdot \nabla \hat{b}|^{-1} = 0.92$ m (evaluated at the outer midplane of the $r/a = 0.8$ flux surface in the left panel of Figure 15), is somewhat smaller than the average radius of curvature $R = 1.51$ m in NCSX. Considering these modifications, the local $R_{loc}/L_{T,loc} = (R_{loc}/R)(a/a_{loc})(R/a)(a/L_T) = 7.39 a/L_T$ in NCSX, while $R/L_T = 3.42 a/L_T$ for a tokamak.

Restating this concern, one may have thought that if NCSX and a tokamak had the same normalized temperature gradient, a/L_T , the ITG modes would be much worse in NCSX due to a much higher $R_{loc}/L_{T,loc}$ than the tokamak. In fact, Figure 12 showed that NCSX has a somewhat higher critical gradient in terms of a/L_T , so the hypothesis that NCSX and a tokamak are similar when expressed in terms of $R_{loc}/L_{T,loc}$ must be incorrect. Indeed, this is strikingly illustrated in Figure 16 (same data as Fig. 12, renormalized), which shows that NCSX has in fact much lower growth rates than a tokamak for the same $R_{loc}/L_{T,loc}$. This is probably because the parallel dynamics are in fact not negligible in NCSX. The eigenfunctions, as seen in Figure 8, are more localized along a field line in NCSX than in a tokamak,

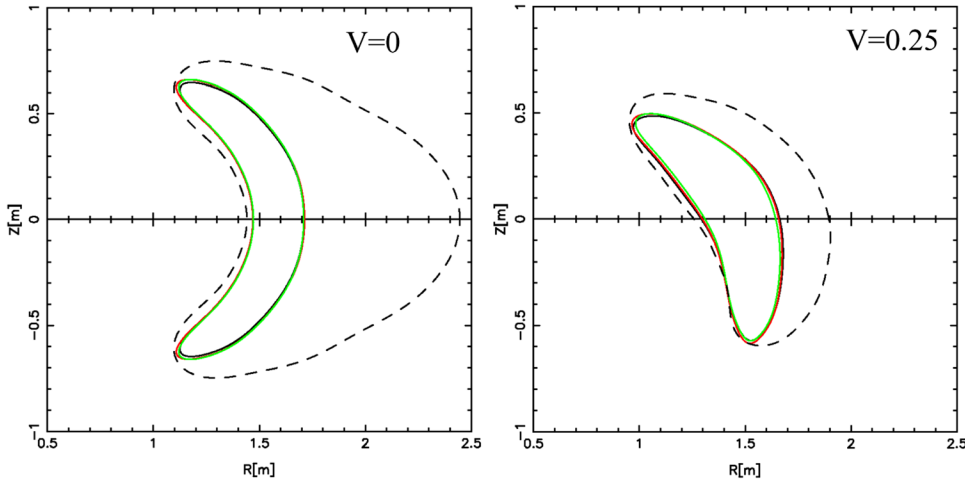


FIG. 15. Poloidal cross sections of NCSX for two toroidal angles. The dashed line is the location of the vacuum vessel and the solid lines are last closed flux surfaces for various ι profiles. Reprinted with permission from Neil Pomphrey *et al.*, PPPL Report PPPL-3701, 2002. More information can be found in Refs. 48 and 49.

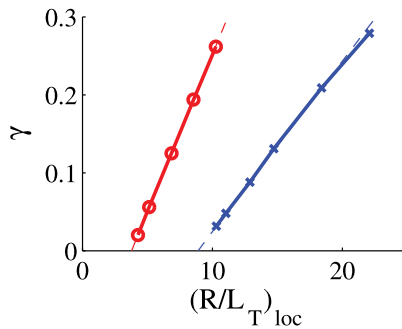


FIG. 16. Similar to Fig. 12, the x-axis is normalized by the local magnetic field radius of curvature R_{loc} , instead of a . This demonstrates that NCSX (blue crosses) performs much better than expected if the instability was the same at the same $(R/L_T)_{loc}$, presumably indicating that additional stabilizing effects in the parallel dynamics are important in NCSX. Tokamak growth rates: red circles.

possibly through some combination of the stabilizing effects of a narrower bad-curvature region (i.e., a shorter connection length between good and bad curvature regions) and stronger local magnetic shear. These effects should be investigated more thoroughly in the future.

III. CONCLUSION

Cross-configuration comparisons of plasma confinement are important to consider for the design of future fusion energy devices. As a simple case, the linear stability of the adiabatic and kinetic ITG modes was compared for NCSX and a tokamak equilibrium. This particular tokamak equilibrium is a composite of JET H-mode shot #52979 and ARIES-AT. NCSX had a similar linear critical temperature gradient $a/L_{T,crit}$ to the tokamak case for ITG modes with adiabatic electrons, although its growth rates were higher than the tokamak's beyond marginal stability. However, for ITG modes with kinetic electrons, NCSX's critical gradient a/L_T is approximately 9% higher than the tokamak's, which would correspond to an approximately 22% increase in the fusion power for NCSX relative to the tokamak. The growth rates in NCSX remained less than for the tokamak until $a/L_T \approx 1.5 a/L_{T,crit}$.

The parameter $a/L_{T,crit}$ is an important figure of merit because it characterizes the core to edge temperature ratio (if the plasma is near marginal stability as expected in typical hot reactor regimes). While the parameter $R/L_{T,crit}$ is often a useful stability parameter in tokamak cases, it was found that stabilizing effects in the parallel dynamics in stellarators can make it a less relevant measure for stellarators. Upon rescaling the kinetic ITG mode data as a function of R/L_T , it was found that NCSX appears even more stable.

Future work that should be done includes using GS2's nonlinear capabilities to compare heat fluxes for various fusion energy devices. Including more physical effects, such as non-zero density gradients and collisionalities, would create a clearer picture of their relative confinement properties. A future study could compare stellarators with tokamaks in various operating regimes that may potentially improve performance further, including reversed magnetic shear and hybrid low-shear scenarios.

ACKNOWLEDGMENTS

The authors wish to thank Neil Pomphrey for creating the NCSX equilibrium, Pavlos Xanthopoulos for the use of and assistance with GIST, and W. Dorland, M. A. Barnes, and W. Guttenfelder for their help with GS2. This work was supported by the U.S. Department of Energy through the SciDAC Center for the Study of Plasma Microturbulence, the Princeton Plasma Physics Laboratory under DOE Contract No. DE-AC02-09CH11466, and Los Alamos National Security, LLC under DOE Contract No. DE-AC52-06NA25396.

¹P. C. Liewer, *Nucl. Fusion* **25**, 543 (1985).

²J. Sapper and H. Renner, *Fusion Technol.* **7**, 62 (1990).

³C. Beidler, G. Grieger, F. Hermann, E. Harmeyer, J. Kisslinger, W. Lotz, H. Maassberg, P. Merkel, J. Nührenberg, F. Rau, J. Sapper, F. Sardei, R. Scardovell, A. Schluter, and H. M. f. P. Woblig, *Fusion Technol.* **17**, 148 (1990).

⁴G. Grieger, W. Lotz, P. Merkel, J. Nührenberg, J. Sapper, E. Strumberger, H. Wobig, R. Burhenn, V. Erckmann, U. Gasparino, L. Giannone, H. J. Hartfuss, R. Jaenicke, G. Kühner, H. Ringler, A. Weller, F. Wagner, W7-X Team, and W7-AS Team, *Phys. Fluids B: Plasma Phys.* **4**, 2081 (1992).

⁵M. C. Zarnstorff, L. A. Berry, A. Brooks, E. Fredrickson, G.-Y. Fu, S. Hirshman, S. Hudson, L.-P. Ku, E. Lazarus, D. Mikkelsen, D. Monticello,

- G. H. Neilson, N. Pomphrey, A. Reiman, D. Spong, D. Strickler, A. Boozer, W. A. Cooper, R. Goldston, R. Hatcher, M. Isaev, C. Kessel, J. Lewandowski, J. F. Lyon, P. Merkel, H. Mynick, B. E. Nelson, C. Nuehrenberg, M. Redi, W. Reiersen, P. Rutherford, R. Sanchez, J. Schmidt, and R. B. White, *Plasma Phys. Controlled Fusion* **43**, A237 (2001).
- ⁶H. Yamada, A. Komori, N. Ohyabu, O. Kaneko, K. Kawahata, K. Y. Watanabe, S. Sakakibara, S. Murakami, K. Ida, R. Sakamoto, Y. Liang, J. Miyazawa, K. Tanaka, Y. Narushima, S. Morita, S. Masuzaki, T. Morisaki, N. Ashikawa, L. R. Baylor, W. A. Cooper, M. Emoto, P. W. Fisher, H. Funaba, M. Goto, H. Idei, K. Ikeda, S. Inagaki, N. Inoue, M. Isobe, K. Khlopenkov, T. Kobuchi, A. Kostrioukov, S. Kubo, T. Kuroda, R. Kumazawa, T. Minami, S. Muto, T. Mutoh, Y. Nagayama, N. Nakajima, Y. Nakamura, H. Nakanishi, K. Narihara, K. Nishimura, N. Noda, T. Notake, S. Ohdachi, Y. Oka, M. Osakabe, T. Ozaki, B. J. Peterson, G. Rewoldt, A. Sagara, K. Saito, H. Sasao, M. Sasao, K. Sato, M. Sato, T. Seki, H. Sugama, T. Shimozuma, M. Shoji, H. Suzuki, Y. Takeiri, N. Tamura, K. Toi, T. Tokuzawa, Y. Torii, K. Tsumori, T. Watanabe, I. Yamada, S. Yamamoto, M. Yokoyama, Y. Yoshimura, T. Watari, Y. Xu, K. Itoh, K. Matsuoka, K. Ohkubo, T. Satow, S. Sudo, T. Uda, K. Yamazaki, O. Motojima, and M. Fujiwara, *Plasma Phys. Controlled Fusion* **43**, A55 (2001).
- ⁷S. P. Gerhardt, J. N. Talmadge, J. M. Canik, and D. T. Anderson, *Phys. Rev. Lett.* **94**, 015002 (2005).
- ⁸J. M. Canik, D. T. Anderson, F. S. B. Anderson, K. M. Likin, J. N. Talmadge, and K. Zhai, *Phys. Rev. Lett.* **98**, 085002 (2007).
- ⁹J. N. Talmadge, F. S. B. Anderson, D. T. Anderson, C. Deng, W. Guttenfelder, K. M. Likin, J. Lore, J. C. Schmitt, and K. Zhai, *Plasma Fusion Res.* **3**, S1002 (2008).
- ¹⁰G. Rewoldt, *Phys. Fluids* **25**, 480 (1982).
- ¹¹G. Rewoldt, W. M. Tang, and R. J. Hastie, *Phys. Fluids* **30**, 807 (1987).
- ¹²G. Rewoldt, L.-P. Ku, W. M. Tang, and W. A. Cooper, *Phys. Plasmas* **6**, 4705 (1999).
- ¹³W. Guttenfelder, J. Lore, D. T. Anderson, F. S. B. Anderson, J. M. Canik, W. Dorland, K. M. Likin, and J. N. Talmadge, *Phys. Rev. Lett.* **101**, 215002 (2008).
- ¹⁴P. Xanthopoulos and F. Jenko, *Phys. Plasmas* **14**, 042501 (2007).
- ¹⁵P. Xanthopoulos, F. Merz, T. Goerler, and F. Jenko, *Phys. Rev. Lett.* **99**, 035002 (2007).
- ¹⁶T.-H. Watanabe, H. Sugama, and S. Ferrando-Margalet, *Nucl. Fusion* **47**, 1383 (2007).
- ¹⁷M. Nunami, T. Watanabe, and H. Sugama, *Plasma Fusion Res.* **5**, 016 (2010).
- ¹⁸J. A. Baumgaertel, E. A. Belli, W. Dorland, W. Guttenfelder, G. W. Hammett, D. R. Mikkelsen, G. Rewoldt, W. M. Tang, and P. Xanthopoulos, *Phys. Plasmas* **18**, 122301 (2011).
- ¹⁹J. A. Baumgaertel, G. W. Hammett, D. R. Mikkelsen, M. Nunami, and P. Xanthopoulos, *Phys. Plasmas* **19**, 122306 (2012).
- ²⁰A. H. Boozer, *Plasma Phys. Controlled Fusion* **50**, 124005 (2008).
- ²¹G. Rewoldt, L.-P. Ku, and W. M. Tang, *Phys. Plasmas* **12**, 102512 (2005).
- ²²M. Nunami, T. H. Watanabe, H. Sugama, and K. Tanaka, *Phys. Plasmas* **19**, 042504 (2012).
- ²³O. Yamagishi, M. Yokoyama, N. Nakajima, and K. Tanaka, *Phys. Plasmas* **14**, 012505 (2007).
- ²⁴T. H. Watanabe, H. Sugama, and S. Ferrando-Margalet, *Phys. Rev. Lett.* **100**, 195002 (2008).
- ²⁵T. H. Watanabe, H. Sugama, and M. Nunami, *Nucl. Fusion* **51**, 123003 (2011).
- ²⁶P. Xanthopoulos, A. Mischchenko, P. Helander, H. S. Sugama, and T. H. Watanabe, *Phys. Rev. Lett.* **107**, 245002 (2011).
- ²⁷W. Dorland, F. Jenko, M. Kotschenreuther, and B. N. Rogers, *Phys. Rev. Lett.* **85**, 5579 (2000).
- ²⁸F. Jenko, W. Dorland, M. Kotschenreuther, and B. N. Rogers, *Phys. Plasmas* **7**, 1904 (2000).
- ²⁹H. E. Mynick, N. Pomphrey, and P. Xanthopoulos, *Phys. Rev. Lett.* **105**, 095004 (2010).
- ³⁰O. Gruber, R. Arslanbekov, C. Atanasiu, A. Bard, G. Becker, W. Becker, M. Beckmann, K. Behler, K. Behringer, A. Bergmann, R. Bilato, D. Bolshukin, K. Borrass, H.-S. Bosch, B. Braams, M. Brambilla, R. Brandenburg, F. Braun, H. Brinkschulte, R. Brueckner, B. Brueschhaber, K. Buechl, A. Buehler, H. Buerbaumer, A. Carlson, M. Ciric, G. Conway, D. P. Coster, C. Dorn, R. Drube, R. Dux, S. Egorov, W. Engelhardt, H.-U. Fahrbach, U. Fantz, H. Faugel, M. Foley, P. Franzen, P. Fu, J. C. Fuchs, J. Gafert, G. Gantenbein, O. Gehre, A. Geier, J. Gernhardt, E. Gubanka, A. Gude, S. Guenter, G. Haas, D. Hartmann, B. Heinemann, A. Herrmann, J. Hobirk, F. Hofmeister, H. Hohenoecker, L. Horton, L. Hu, D. Jacobi, M. Jakobi, F. Jenko, A. Kallenbach, O. Kardaun, M. Kaufmann, A. Kendl, J.-W. Kim, K. Kirov, R. Kochergov, H. Kollotzek, W. Kraus, K. Krieger, B. Kurzan, G. Kyriakakis, K. Lackner, P. T. Lang, R. S. Lang, M. Laux, L. Lengyel, F. Leuterer, A. Lorenz, H. Maier, K. Mank, M.-E. Manso, M. Maraschek, K.-F. Mast, P. J. McCarthy, D. Meisel, H. Meister, F. Meo, R. Merkel, V. Mertens, J. P. Meskat, R. Monk, H. W. Mueller, M. Muenich, H. Murrmann, G. Neu, R. Neu, J. Neuhauser, J.-M. Noterdaeme, I. Nunes, G. Pautasso, A. G. Peeters, G. Pereverzev, S. Pinches, E. Poli, R. Pugno, G. Raupp, T. Ribeiro, R. Riedl, S. Riondato, V. Rohde, H. Roehr, J. Roth, F. Ryter, H. Salzmann, W. Sandmann, S. Sarelma, S. Schade, H.-B. Schilling, D. Schloegl, K. Schmidtman, R. Schneider, W. Schneider, G. Schramm, J. Schweinzer, S. Schweizer, B. D. Scott, U. Seidel, F. Serra, S. Sesnic, C. Sihler, A. Silva, A. Sips, E. Speth, A. Staebler, K.-H. Steuer, J. Stober, B. Streibl, E. Strumberger, W. Suttrop, A. Tabasso, A. Tanga, G. Tardini, C. Tichmann, W. Treutterer, M. Troppmann, N. Tsois, W. Ullrich, M. Ullrich, P. Varela, O. Vollmer, U. Wenzel, F. Wesner, R. Wolf, E. Wolfrum, R. Wunderlich, N. Xanthopoulos, Q. Yu, M. Zarrabian, D. Zasche, T. Zehetbauer, H.-P. Zehrfeld, A. Zeiler, and H. Zohm, *Nucl. Fusion* **41**, 1369 (2001).
- ³¹H. E. Mynick, N. Pomphrey, and P. Xanthopoulos, *Phys. Plasmas* **18**, 056101 (2011).
- ³²G. Staebler and H. S. John, *Nucl. Fusion* **46**, L6 (2006).
- ³³A. M. Dimits, G. Bateman, M. A. Beer, B. I. Cohen, W. Dorland, G. W. Hammett, C. Kim, J. E. Kinsey, M. Kotschenreuther, A. H. Kritz, L. L. Lao, J. Mandrekas, W. M. Nevins, S. E. Parker, A. J. Redd, D. E. Shumaker, R. Sydora, and J. Weiland, *Phys. Plasmas* **7**, 969 (2000).
- ³⁴F. Jenko, W. Dorland, and G. W. Hammett, *Phys. Plasmas* **8**, 4096 (2001).
- ³⁵E. A. Belli, G. W. Hammett, and W. Dorland, *Phys. Plasmas* **15**, 092303 (2008).
- ³⁶F. Najmabadi, A. Abdou, L. Bromberg, T. Brown, V. Chan, M. Chu, F. Dahlgren, L. El-Guebaly, P. Heitzenroeder, D. Henderson, H. St. John, C. Kessel, L. Lao, G. Longhurst, S. Malang, T. Mau, B. Merrill, R. Miller, E. Mogahed, R. Moore, T. Petrie, D. Petti, P. Politzer, A. Raffray, D. Steiner, I. Sviatoslavsky, P. Synder, G. Staebler, A. Turnbull, M. Tillack, L. Waganer, X. Wang, P. West, and P. Wilson, *Fusion Eng. Design* **80**, 3 (2006).
- ³⁷E. A. Lazarus, M. S. Chu, J. R. Ferron, F. J. Helton, J. T. Hogan, A. G. Kellman, L. L. Lao, J. B. Lister, T. H. Osborne, R. Snider, E. J. Strait, T. S. Taylor, and A. D. Turnbull, *Phys. Fluids B: Plasma Phys.* **3**, 2220 (1991).
- ³⁸E. J. Strait, *Phys. Plasmas* **1**, 1415 (1994).
- ³⁹D. A. Gates, *Phys. Plasmas* **10**, 1659 (2003).
- ⁴⁰C. Roach, M. Walters, R. Budny, F. Imbeaux, T. Fredian, M. Greenwald, J. Stillerman, D. Alexander, J. Carlsson, J. Cary, F. Ryter, J. Stober, P. Gohil, C. Greenfield, M. Murakami, G. Bracco, B. Esposito, M. Romanelli, V. Parail, P. Stubberfield, I. Voitsekhovitch, C. Brickley, A. Field, Y. Sakamoto, T. Fujita, T. Fukuda, N. Hayashi, G. Hogewij, A. Chudnovskiy, N. Kinerva, C. Kessel, T. Aniel, G. Hoang, J. Ongena, E. Doyle, W. Houlberg, A. Polevoi, ITPA Confinement Database and Modelling Topical Group, and ITPA Transport Physics Topical Group, *Nucl. Fusion* **48**, 125001 (2008).
- ⁴¹M. Valovic, J. Rapp, J. G. Cordey, R. Budny, D. C. McDonald, L. Garzotti, A. Kallenbach, M. A. Mahdavi, J. Ongena, V. Parail, G. Saibene, R. Sartori, M. Stamp, O. Sauter, J. Strachan, W. Suttrop, and c. t. t. E. Workprogramme, *Plasma Phys. Controlled Fusion* **44**, 1911 (2002).
- ⁴²J. Ongena, P. Monier-Garbet, W. Suttrop, P. Andrew, M. Bécoulet, R. Budny, Y. Corre, G. Cordey, P. Dumortier, T. Eich, L. Garzotti, D. Hillis, J. Hogan, L. Ingesson, S. Jachmich, E. Joffrin, P. Lang, A. Loarte, P. Lomas, G. Maddison, D. McDonald, A. Messiaen, M. Nave, G. Saibene, R. Sartori, O. Sauter, J. Strachan, B. Unterberg, M. Valovic, I. Voitsekhovitch, M. v. Hellermann, B. Alper, Y. Baranov, M. Beurskens, G. Bonheure, J. Brzozowski, J. Bucalossi, M. Brix, M. Charlet, I. Coffey, M. D. Baar, P. D. Vries, C. Giroud, C. Gowers, N. Hawkes, G. Jackson, C. Jupen, A. Kallenbach, H. Koslowski, K. Lawson, M. Mantsinen, G. Matthews, F. Milani, M. Murakami, A. Murari, R. Neu, V. Parail, S. Podda, M. Puiatti, J. Rapp, E. Righi, F. Sartori, Y. Sarazin, A. Staebler, M. Stamp, G. Telasca, M. Valisa, B. Weyssow, K. Zastrow, and E. W. Contributors, *Nucl. Fusion* **44**, 124 (2004).
- ⁴³R. L. Miller, M. S. Chu, J. M. Greene, Y. R. Lin-Liu, and R. E. Waltz, *Phys. Plasmas* **5**, 973 (1998).
- ⁴⁴J. A. Baumgaertel, "Simulating the effects of stellarator geometry on gyrokinetic drift-wave turbulence," Ph.D. dissertation (Princeton University, 2012).

- ⁴⁵M. Barnes, "Trinity: A unified treatment of turbulence, transport, and heating in magnetized plasmas," Ph.D. dissertation (University of Maryland, 2009).
- ⁴⁶D. R. Mikkelsen and W. Dorland, *Phys. Rev. Lett.* **101**, 135003 (2008).
- ⁴⁷J. L. Peterson, R. Bell, J. Candy, W. Guttenfelder, G. W. Hammett, S. M. Kaye, B. LeBlanc, D. R. Mikkelsen, D. R. Smith, and H. Y. Yuh, *Phys. Plasmas* **19**, 056120 (2012).
- ⁴⁸N. Pomphrey, R. Hatcher, S. P. Hirshman, S. Hudson, L. Ku, E. Lazarus, H. Mynick, D. Monticello, G. H. Neilson, A. Reiman, and NCSX Team, PPPL Report PPPL-3701, 2002.
- ⁴⁹N. Pomphrey, A. Boozer, A. Brooks, R. Hatcher, S. P. Hirshman, S. Hudson, L. Ku, E. Lazarus, H. Mynick, D. Monticello, M. Redi, A. Reiman, M. C. Zarnstorff, and I. Zatz, *Fusion Sci. Technol.* **51**, 181 (2007).